Electronic Supplementary Information

New porous coordination polymer reveals selective sensing of Fe^{3+}, $Cr_2O_7^{2-}$, CrO_4^{2-}, MnO_4^- and nitrobenzene, and stimuli-responsive luminescent color conversions

Bin Li, Qing-Qing Yan and Guo-Ping Yong*
Department of Chemistry, University of Science and Technology of China, Hefei 230026, P. R. China
E-mail: gpyong@ustc.edu.cn

Table S1 The loading amounts of Fe^{3+} or $Cr_2O_7^{2-}$ in USTC-5.

concentrations	3×10^{-4} M	5×10^{-4} M	8×10^{-4} M	1×10^{-3} M	3×10^{-3} M
loading amounts of Fe^{3+} (μg/mg)	1.15	1.61	1.88	1.90	2.03
loading amounts of $Cr_2O_7^{2-}$ (μg/mg)	0.118	0.150	0.200	0.225	0.288

Table S2 Selected bond distances (Å) and angles (°) for USTC-5.

USTC-5	
Zn(1)-O(1)	2.130(2)
Zn(1)-O(2)	2.212(2)
Zn(1)-O(3)	2.354(2)
Zn(1)-O(4)	2.0776(17)
Zn(1)-N(1)	2.0702(17)
Zn(1)-N(5)	2.0806(18)
O(1)-Zn(1)-O(2)	59.56(7)
O(1)-Zn(1)-O(3)	97.99(8)
O(1)-Zn(1)-O(4)	99.52(8)
O(1)-Zn(1)-N(1)	152.85(8)
O(1)-Zn(1)-N(5)	90.65(8)
O(2)-Zn(1)-O(3)	101.64(7)
O(2)-Zn(1)-O(4)	150.74(8)
O(2)-Zn(1)-N(1)	93.34(7)
O(2)-Zn(1)-N(5)	105.23(8)
O(3)-Zn(1)-O(4)	58.45(7)
O(3)-Zn(1)-N(1)	85.26(8)
O(3)-Zn(1)-N(5)	152.50(7)
O(4)-Zn(1)-N(1)	104.98(7)
O(4)-Zn(1)-N(5)	94.46(7)
N(1)-Zn(1)-N(5)	98.82(7)

Table S3 The comparison this work with recently published articles related to sensing

analytes	MOFs	solvents	quenching constants K_{sv} (M^{-1})	detection limits （μM）	references
Fe^{3+}	$\{[Zn_2(TRZ)_2(DBTDC\text{-}O_2)]\cdot DMA\}_n$	H_2O	1.01×10^4	4.61	[1]
	USTC-5	H_2O	9.85×10^3	1.91	*This Work*
	$[Zn_2(NO_3)_2(4,4'\text{-bpy})_2(TBA)]_n$	H_2O	7.48×10^3	7.18	[2]
	$[Zn_2(cptpy)(btc)(H_2O)]_n$	H_2O	5.46×10^3	4.33	[3]
	$\{[Zn_3(HL1)_2H_2O]\cdot 4H_2O\}_n$	H_2O	5.00×10^3	220	[4]
	$\{[Me_2NH_2]\text{-}[Zn_2(HEDP)(BPDC)_{0.5}(H_2O)_2]\cdot H_2O\}_n$	H_2O	4.74×10^3	NM	[5]
$Cr_2O_7^{2-}$	$[Cd(L2)_2(H_2O)_2]_n$	H_2O	5.10×10^4	34.1	[6]
	USTC-5	H_2O	1.25×10^4	1.45	*This Work*
	$\{[Zn_2(TRZ)_2(DBTDC\text{-}O_2)]\cdot DMA\}_n$	H_2O	1.24×10^4	2.55	[1]
	$[Zn(L3)(BBI)\cdot(H_2O)_2]_n$	H_2O	1.17×10^4	NM	[7]
	$\{[Zn_2(TPOM)(NH_2\text{–}BDC)_2]\cdot 4H_2O\}_n$	DMF	7.59×10^3	3.9	[8]
	$[Zn(btz)]_n$	H_2O	4.23×10^3	NM	[9]
CrO_4^{2-}	**USTC-5**	H_2O	1.34×10^4	11.4	*This Work*
	$\{[Zn_3(L4)(OH)(H_2O)_5]\cdot NMP\cdot 2H_2O\}_n$	H_2O	1.30×10^4	429	[10]
	$[Cd(L2)_2(H_2O)_2]_n$	H_2O	1.10×10^4	175	[6]
	$\{[Zn_2(TPOM)(NH_2\text{–}BDC)_2]\cdot 4H_2O\}_n$	DMF	4.45×10^3	4.8	[8]
	$[Zn(btz)]_n$	H_2O	3.19×10^3	NM	[9]
	$\{[Eu(L5)(H_2O)_2]\cdot 5H_2O\}_n$	H_2O	1.74×10^3	NM	[11]
MnO_4^-	$\{[Tb(TBOT)(H_2O)]\cdot 4H_2O\cdot DMF\cdot 0.5NMP\}_n$	H_2O	6.63×10^4	340	[12]
	USTC-5	H_2O	1.92×10^4	23.4	*This Work*
	$\{[Zn_3(L4)(OH)(H_2O)_5]\cdot NMP\cdot 2H_2O\}_n$	H_2O	1.10×10^4	338	[10]
	$[Ba_3La_{0.5}(\mu_3\text{-}L6)_{2.5}(H_2O)_3(DMF)]\cdot 3DMF\}_n$	H_2O	7.73×10^3	0.28	[13]
	$\{[Cd(L7)(glu)]\cdot 3H_2O\}_n$	DMF	4.53×10^3	4.64	[14]
	$\{[Eu(L5)(H_2O)_2]\cdot 5H_2O\}_n$	H_2O	5.10×10^2	NM	[11]
NB	$\{[Me_2NH_2]\text{-}[Cd_2(L8)(DMA)]\}_n$	DMA	2700	2540	[15]
	$\{[Tb(L9)_{1.5}(H_2O)]\cdot 4H_2O\}_n$	EtOH	2270	4.00	[16]
	$\{[Eu_2(L10)_2(DMA)_2]\cdot nH_2O\}_n$	DMA	1390	1200	[17]
	USTC-5	DMF	770	12.0	*This Work*
	$\{[Me_2NH_2]\text{-}[Zn_2(L11)(H_2O)]\cdot 6DMF\cdot 4H_2O\}_n$	DMF	564	NM	[18]
	$\{[Zn_4(L12)_3O]\cdot 8DMF\cdot H_2O\}_n$	DMF	155	NM	[19]

NM = No Mention

HTRZ = 1,2,4-triazole; $H_2DBTDC-O_2$ = S,S-dioxodibenzothiophen-3,7-dicarboxylic acid; 4,4'-bpy = 4,4'-bipyridine; H_2TBA = 4-(1*H*-tetrazol-5-yl)-benzoic acid; Hcptpy=4-(4-carboxyphenyl)-2,2':4',4''-terpyridine; H_3btc=1,3,5-benzenetricarboxylic acid; HEDP = 1-hydroxyethylidene diphosphonate; H_2BPDC = biphenyl-4,4'-dicarboxylic acid; BBI = 1,1'-(1,4-butanediyl)bis(imidazole); TPOM = tetrakis(4-pyridyloxymethylene)methane; NH_2–BDC = 2-aminoterephthalic acid; H_2btz = 1,5-bis(5-tetrazolo)-3-oxapentane; H_3TBOT = 2,4,6-tris[1-(3-carboxylphenoxy)ylmethyl]mesitylene; H_2glu = glutaric acid; H_4L1 = 1-(3,5-dicarboxylatobenzyl)-3,5-pyrazole dicarboxylic acid; HL2 = 5-(triazol-1-yl)nicotinic acid;

H_2L3 = benzo-(1,2;4,5)-bis(thiophene-2'-carboxylic acid; H_5L4 = 2,4-di(3',5'-dicarboxylphenyl benzoic acid);

$H_4L5^+Cl^-$ = 1,3-bis(3,5-dicarboxyphenyl) imidazolium chloride; H_3L6 = *p*-terphenyl-3,4'',5-tricarboxylic acid;

L7 = pyridine-3,5-bis(5-azabenzimidazole); H_5L8 = 2,4-di(3',5'-dicarboxylphenyl) benzoic acid; H_2L9 = 2-(1*H*-1,2,4-triazol-1-yl)terephthalic acid; H_4L10 = 5-(bis(4-carboxybenzyl)amino)-isophthalic acid;

H_5L11 = 5,5'-(6-(4-carboxyphenylamino)-1,3,5-triazine-2,4- diyldiimino) diisophthalic acid; H_2L12 = 2,6-bis(4'-carboxyl-phenyl)pyridine.

References

[1] He H M, Du M, et al. Design of a highly-stable pillar-layer zinc(II) porous framework for rapid, reversible, and multi-responsive luminescent sensor in water [J]. *Cryst. Growth Des.* **2019**, *19*, 694−703.

[2] Zhang X, Zhuang X R, et al. A luminescent sensor based on a Zn(II) coordination polymer for selective and sensitive detection of NACs and Fe^{3+} ions [J]. *CrystEngComm* **2019**, *21*, 1948−1955.

[3] Chen H J, Zhang S W, et al. A bifunctional luminescent metal–organic framework for the sensing of paraquat and Fe^{3+} ions in water [J]. *Chem. Asian J.* **2019**, *14*, 3611−3619.

[4] Liu W N, Wang Y Y, et al. Five new 3D transition MOFs based on 1-(3,5-dicarboxylatobenzyl)-3,5-pyrazole dicarboxylic acid displaying unique luminescence sensing towards Fe^{3+} and magnetic properties [J]. *Dalton Trans.* **2019**, *48*, 7786−7793.

[5] Liu H H, Wang G M, et al. Multiple detection characteristics of two zinc phosphonates: Syntheses, crystal structures, and luminescent properties [J]. *Cryst. Growth Des.* **2019**, *19*, 5326−5333.

[6] Yan Y T, Wang Y Y, et al. Seven luminescent metal–organic frameworks constructed from 5-(triazol-1-yl)nicotinic acid: luminescent sensors for Cr^{VI} and MnO_4^- ions in an aqueous medium [J]. *New J. Chem.* **2018**, *42*, 9865−9875.

[7] Zhao Y, Wen L L, et al. Metal−organic frameworks constructed from a new thiophene-functionalized dicarboxylate: Luminescence sensing and pesticide removal [J]. *ACS Appl. Mater. Interfaces* **2017**, *9*, 15164−15175.

[8] Lv R, Liu X, et al. An amino-decorated dual-functional metal–organic framework for highly selective sensing of Cr(III) and Cr(VI) ions and detection of nitroaromatic explosives [J]. *J. Mater. Chem. A.* **2016**, *4*, 15494−15500.

[9] Cao C S, Zhao B, et al. Two solvent-stable MOFs as a recyclable luminescent probe for

detecting dichromate or chromate anions [J]. *CrystEngComm* **2016**, *18*, 4445−4451.
[10] Yan Y T, Hou L, et al. Four new metal–organic frameworks based on diverse secondary building units: Sensing and magnetic properties [J]. *Dalton Trans.* **2018**, *47*, 1682−1692.
[11] Zhang P F, Wang Y Y, et al. Series of water-stable lanthanide metal−organic frameworks based on carboxylic acid imidazolium chloride: Tunable luminescent emission and sensing [J]. *Inorg. Chem.* **2019**, *58*, 13969−13978.
[12] Chen M, Du M, et al. A terbium(III) lanthanide–organic framework as a platform for a recyclable multi-responsive luminescent sensor [J]. *J. Mater. Chem. C.* **2017**, *5*, 2015−2021.
[13] Ding B, Li Y, et al. Heterometallic alkaline earth−lanthanide Ba^{II}−La^{III} microporous metal−organic framework as bifunctional luminescent probes of Al^{3+} and MnO_4^- [J]. *Inorg. Chem.* **2016**, *55*, 4391−4402.
[14] Chen Y Q, Bian Y J, et al. Cd^{II}–organic frameworks fabricated with a N-rich ligand and flexible dicarboxylates: Structural diversity and multi-responsive luminescent sensing for toxic anions and ethylenediamine [J]. *Chem. Asian J.* **2019**, *14*, 4420−4428.
[15] Yan Y T, Zhang W Y, et al. Highly selective luminescence sensing for the detection of nitrobenzene and Fe^{3+} by new Cd(II)-based MOFs [J]. *CrystEngComm* **2018**, *20*, 477−486.
[16] Li Z J, Wang Y Y, et al. Tunable emission and selective luminescence sensing in a series of lanthanide metal−organic frameworks with uncoordinated Lewis basic triazolyl sites [J]. *Cryst. Growth Des.* **2018**, *18*, 2031−2039.
[17] Wang X Y, Li G M, et al. Highly efficient white-light emission and UV-visible/NIR luminescence sensing of lanthanide metal−organic frameworks [J]. *Cryst. Growth Des.* **2017**, *17*, 2178−2185.
[18] Dai Y, Wang H L, et al. Two (5,5)-connected isomeric frameworks as highly selective and sensitive photoluminescent probes of nitroaromatics [J]. *CrystEngComm* **2017**, *19*, 2786−2794.
[19] Wu D, Wang Y Y, et al. New doubly interpenetrated MOF with $[Zn_4O]$ clusters and its doped isomorphic MOF: Sensing, dye, and gas adsorption capacity [J]. *Cryst. Growth Des.* **2019**, *19*, 6774−6783.

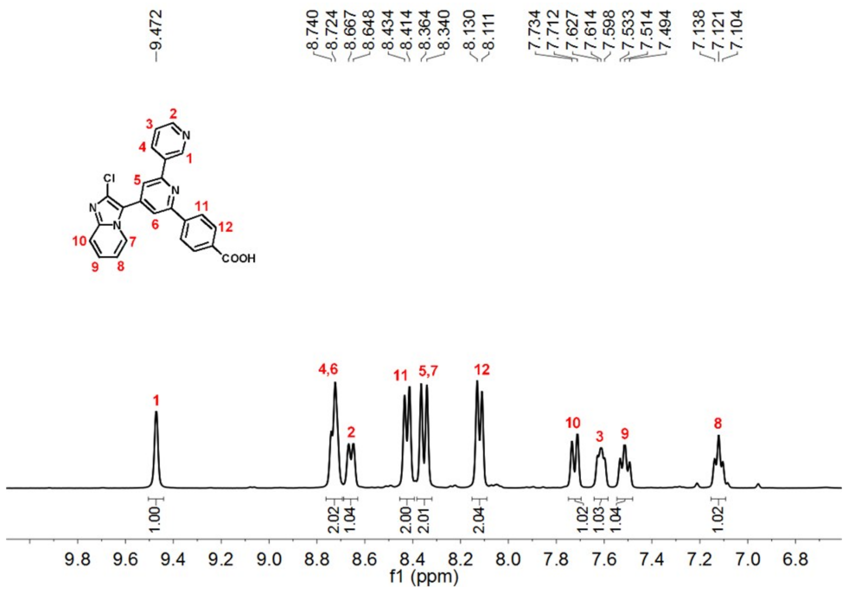

Fig. S1 ^{1}H NMR (400 MHz, dmso-d_6) of HL ligand.

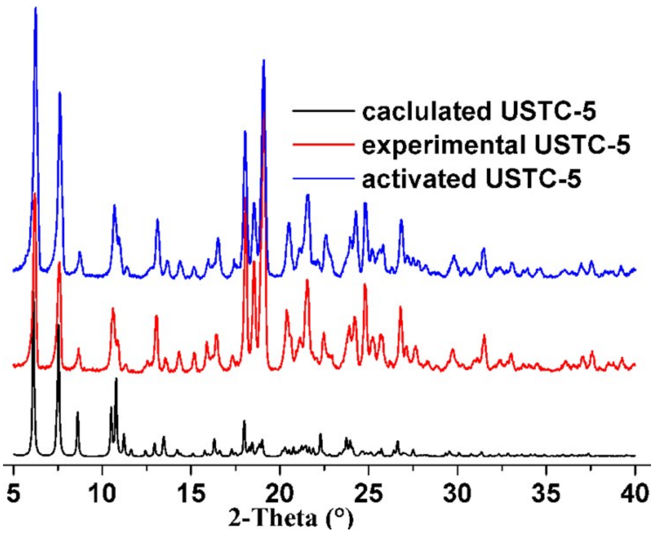

Fig. S2 Powder XRD profiles of calculated and experimental USTC-5, and activated USTC-5.

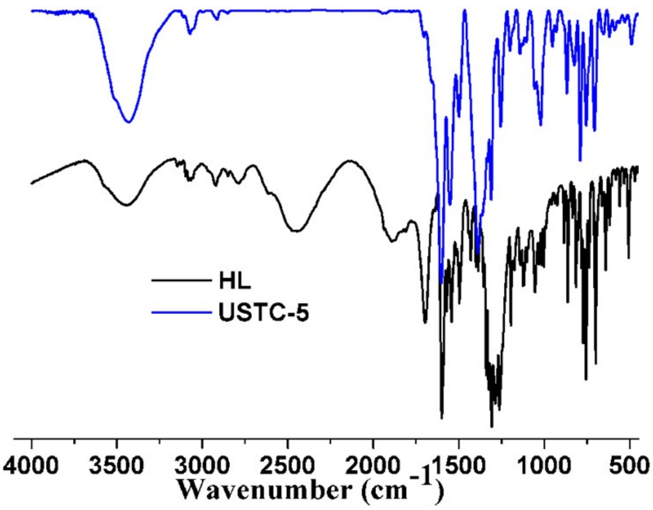

Fig. S3 IR absorption of HL ligand and USTC-5.

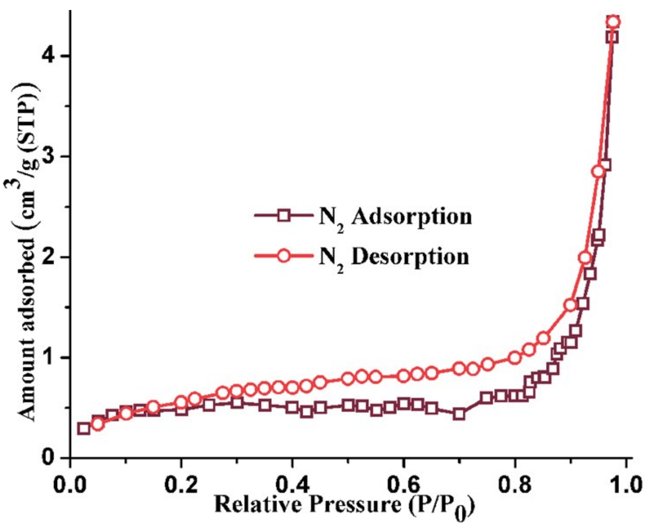

Fig. S4 The N_2 gas adsorption isotherms at 77 K for activated USTC-5.

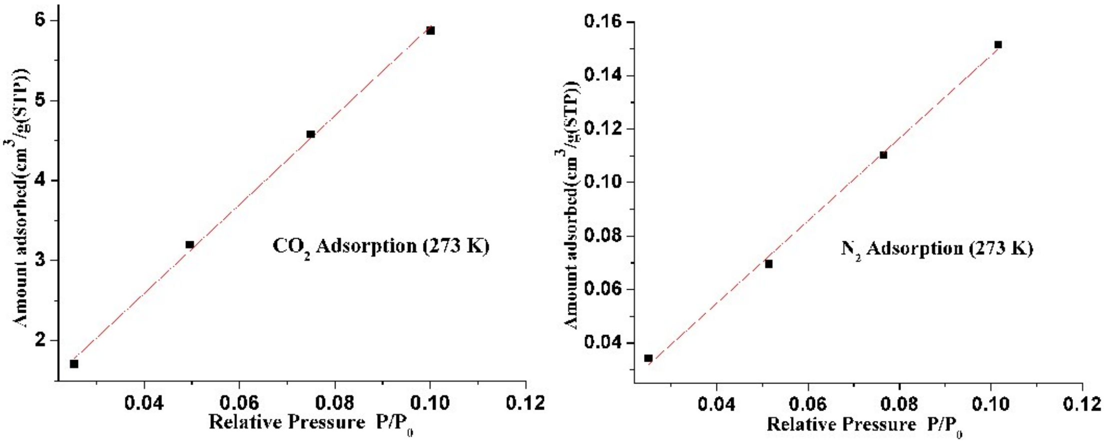

Fig. S5 The Henry's constants (K_H) of CO_2 and N_2 gases at 273 K for USTC-5.

For this method, it should be kept in mind that the ratio of the Henry's law constants will reflect the real mixture selectivity only at very low pressure and low loadings on the adsorbent.

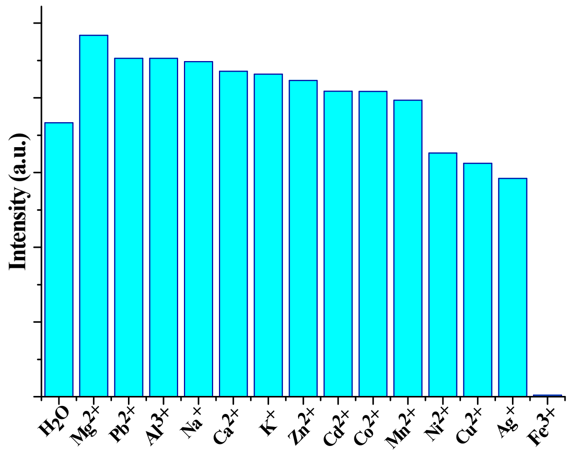

Fig. S6 The bar chart of luminescent intensities at maximum emission wavelength (*ca.* 436 nm) of USTC-5 suspended in different metal ion aqueous solutions.

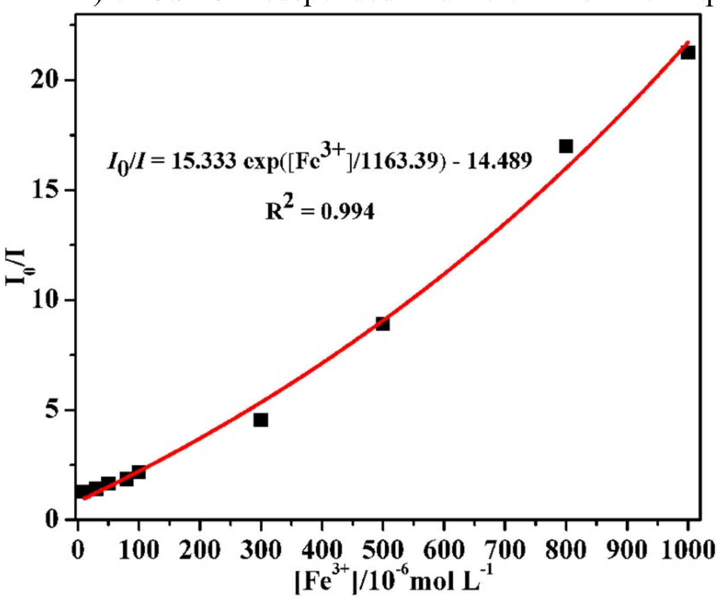

Fig. S7 Plot of I_0/I versus concentration of Fe^{3+} ion aqueous solutions.

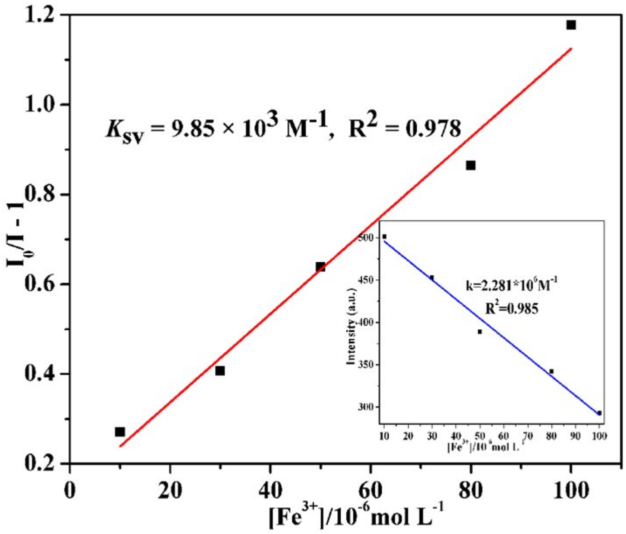

Fig. S8 Stern–Volmer plot of $I_0/I-1$ versus concentration of Fe^{3+} ion aqueous solutions. Inset: luminescent intensity versus concentration of Fe^{3+} ion aqueous solutions.

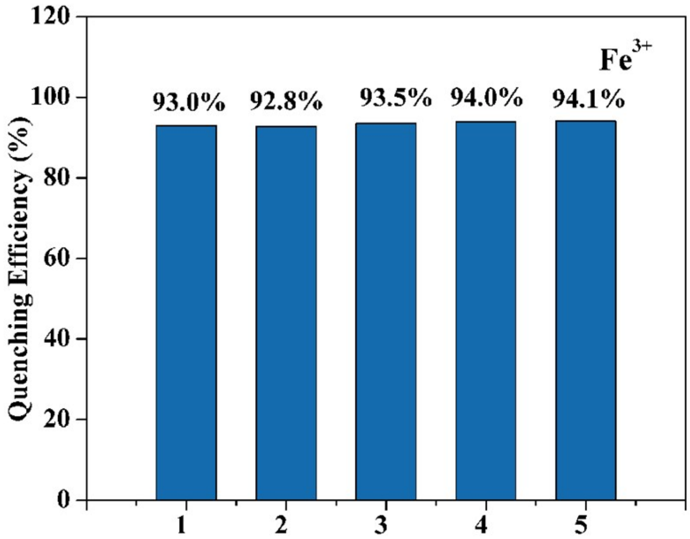

Fig. S9 Quenching efficiencies of USTC-5 in recyclable experiments for Fe^{3+}.

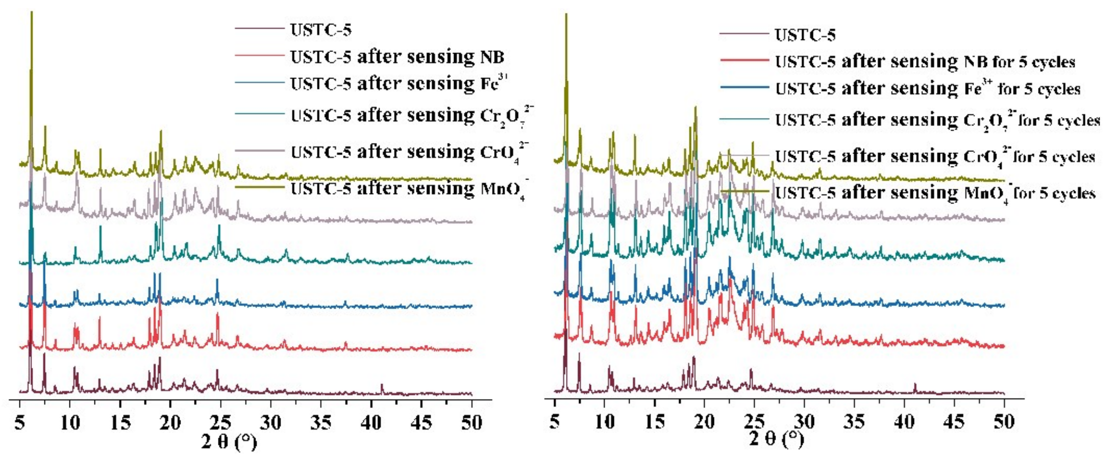

Fig. S10 PXRD patterns of USTC-5 treated by NB's DMF solution, $Fe(NO_3)_3$, $K_2Cr_2O_7$, K_2CrO_4 and $KMnO_4$ aqueous solutions, indicating that USTC-5 retains its framework after immersed in different solutions containing NB molecules or ions (left), and even after 5 sensing cycles (right).

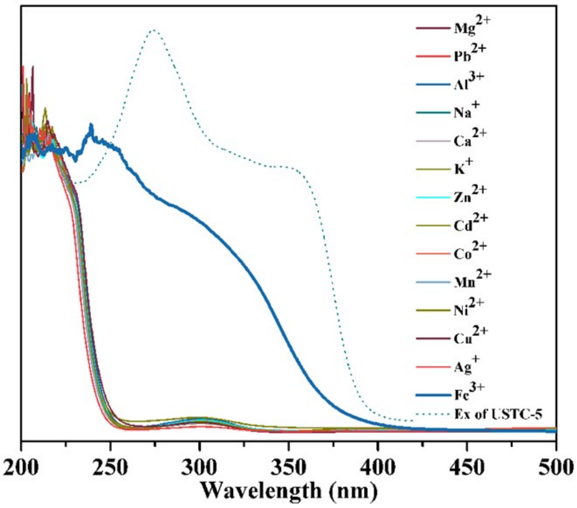

Fig. S11 UV-vis adsorption spectra of different $M(NO_3)_X$ aqueous solutions, and the excitation spectrum of USTC-5.

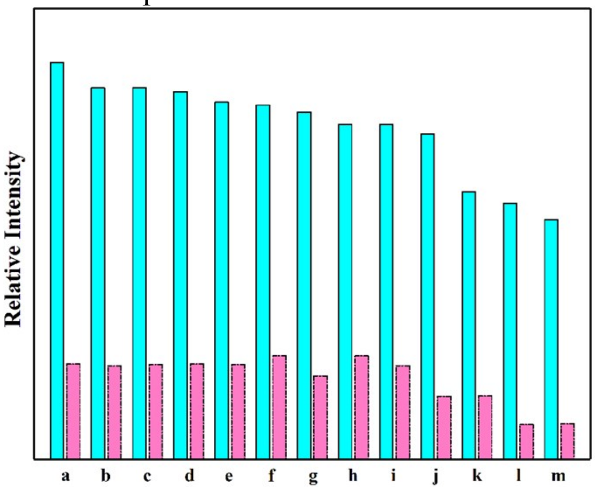

Fig. S12 The bar chart of luminescent intensities at maximum emission wavelength (*ca.* 436 nm) of USTC-5 suspended in 0.01 M interfering ion aqueous solutions (blue-green), and in the mixed aqueous solutions including 7.5×10^{-3} M interfering ion and 2.5×10^{-4} M Fe^{3+} ion (pink). The interfering ion: Mg^{2+}(a), Pb^{2+}(b), Al^{3+}(c), Na^{+}(d), Ca^{2+}(e), K^{+}(f), Zn^{2+}(g), Cd^{2+}(h), Co^{2+}(i), Mn^{2+}(j), Ni^{2+}(k), Cu^{2+}(l) or Ag^{+}(m).

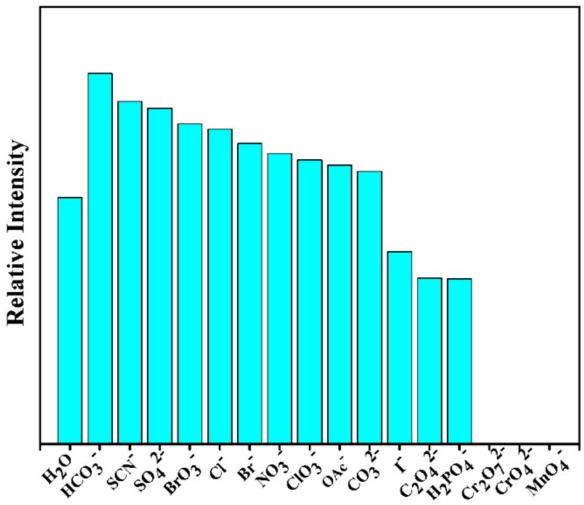

Fig. S13 The bar chart of luminescent intensities at maximum emission wavelength (*ca.* 436 nm) of USTC-5 suspended in different anionic aqueous solutions.

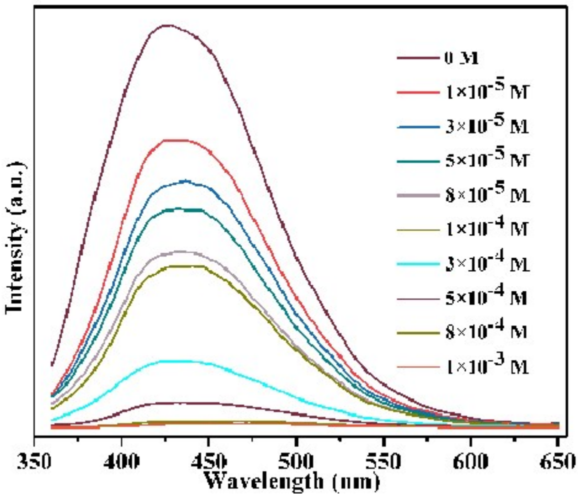

Fig. S14 Luminescence spectra of USTC-5 dispersed in various concentrations of $Cr_2O_7^{2-}$ aqueous solutions.

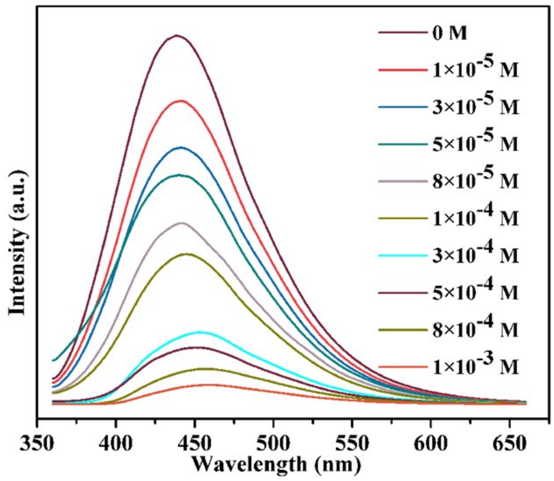

Fig. S15 Luminescence spectra of USTC-5 dispersed in various concentrations of CrO_4^{2-} aqueous solutions.

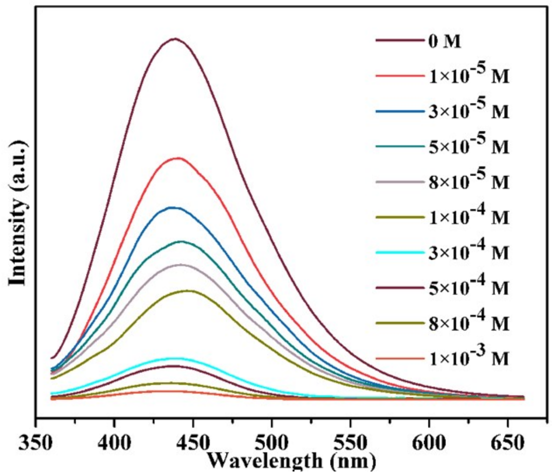

Fig. S16 Luminescence spectra of USTC-5 dispersed in various concentrations of MnO_4^- aqueous solutions.

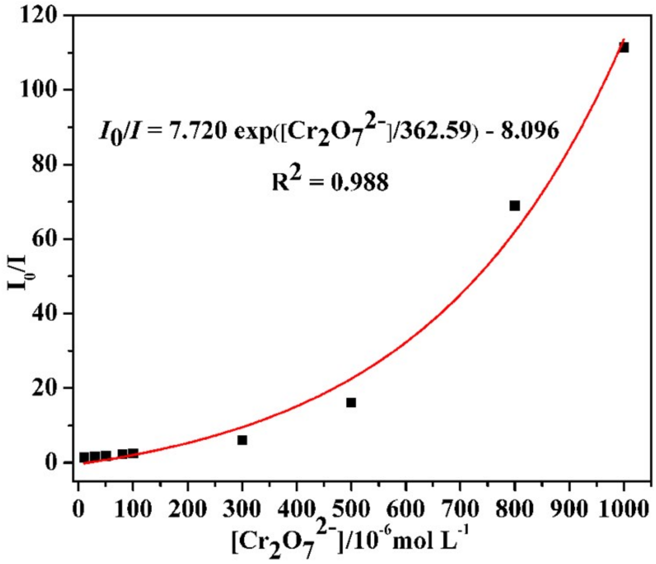

Fig. S17 Plot of I_0/I versus concentration of $Cr_2O_7^{2-}$ ion aqueous solutions.

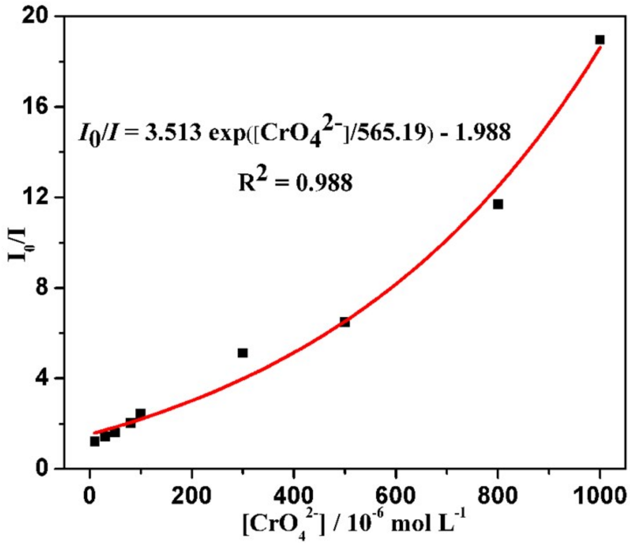

Fig. S18 Plot of I_0/I versus concentration of CrO_4^{2-} ion aqueous solutions.

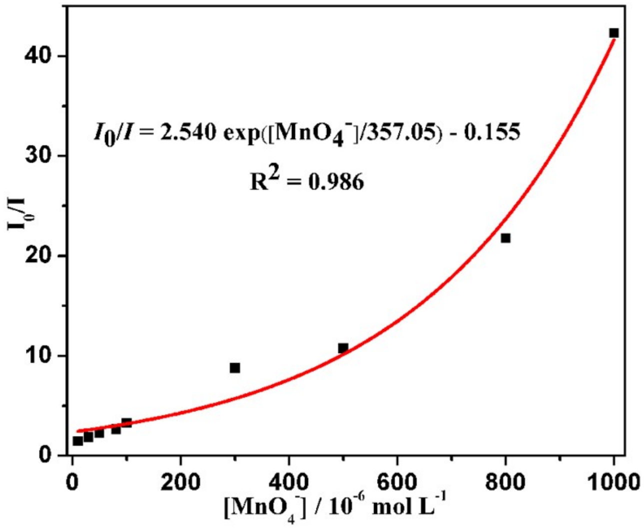

Fig. S19 Plot of I_0/I versus concentration of MnO_4^- ion aqueous solutions.

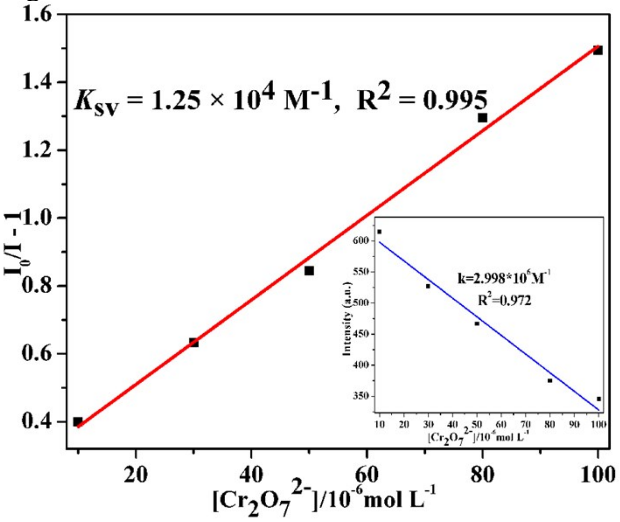

Fig. S20 Stern–Volmer plot of I_0/I−1 versus concentration of $Cr_2O_7^{2-}$ ion aqueous solutions. Inset: luminescent intensity versus concentration of $Cr_2O_7^{2-}$ ion aqueous solutions.

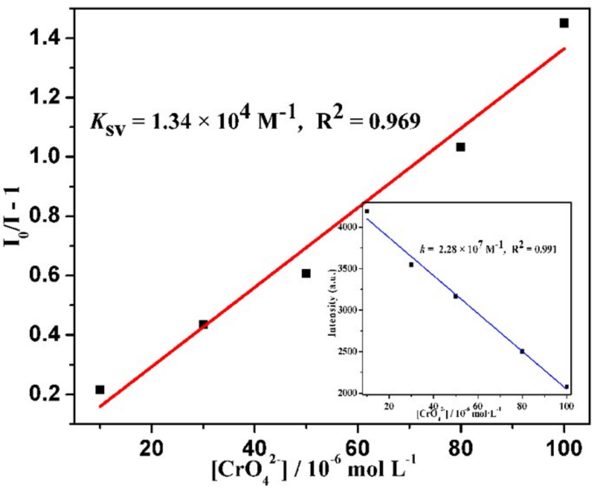

Fig. S21 Stern–Volmer plot of I_0/I−1 versus concentration of CrO_4^{2-} ion aqueous solutions. Inset: luminescent intensity versus concentration of CrO_4^{2-} ion aqueous solutions.

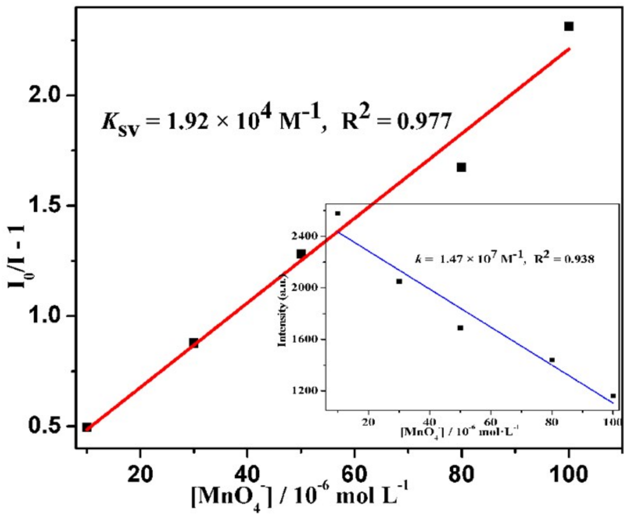

Fig. S22 Stern–Volmer plot of $I_0/I-1$ versus concentration of MnO_4^- ion aqueous solutions. Inset: luminescent intensity versus concentration of MnO_4^- ion aqueous solutions.

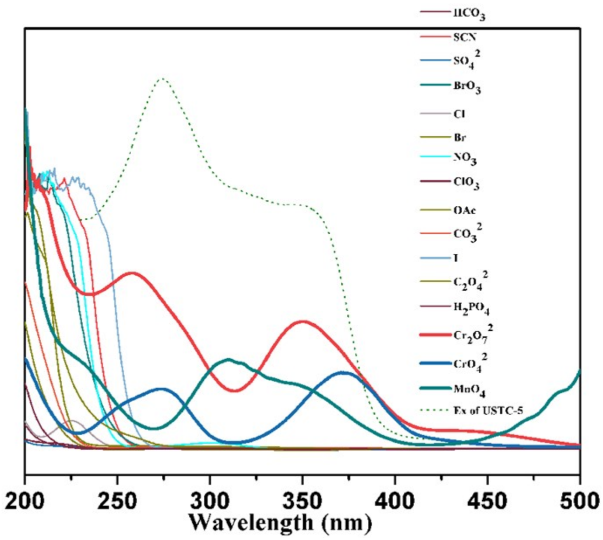

Fig. S23 UV-vis adsorption spectra of different K_yA aqueous solutions, and the excitation spectrum of USTC-5.

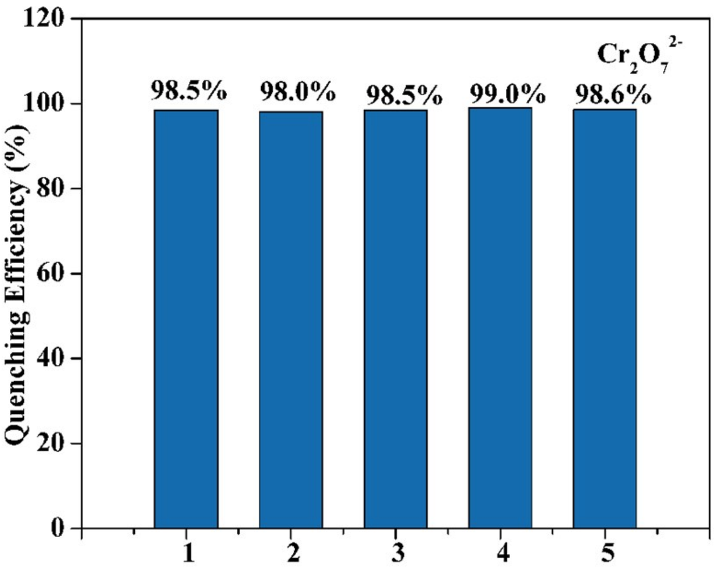

Fig. S24 Quenching efficiencies of USTC-5 in recyclable experiments for $Cr_2O_7^{2-}$.

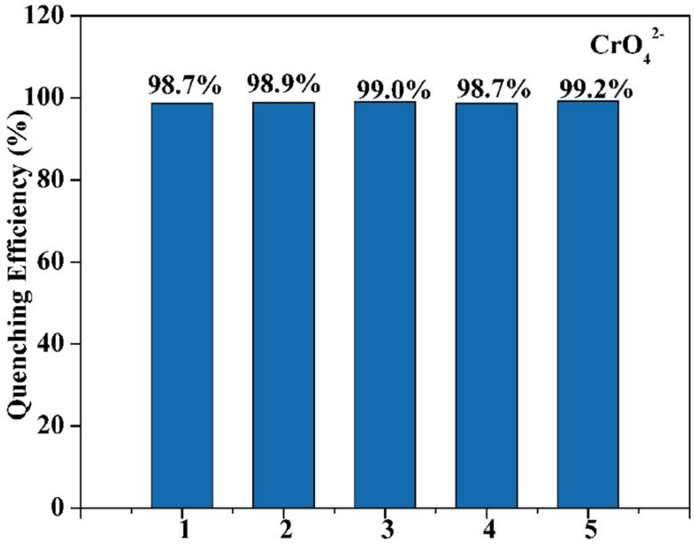

Fig. S25 Quenching efficiencies of USTC-5 in recyclable experiments for CrO_4^{2-}.

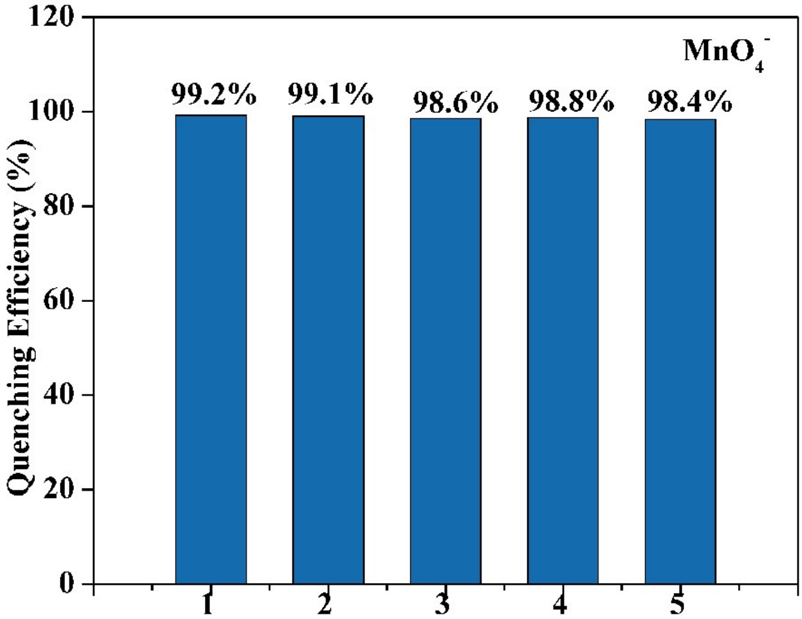

Fig. S26 Quenching efficiencies of USTC-5 in recyclable experiments for MnO_4^{-}.

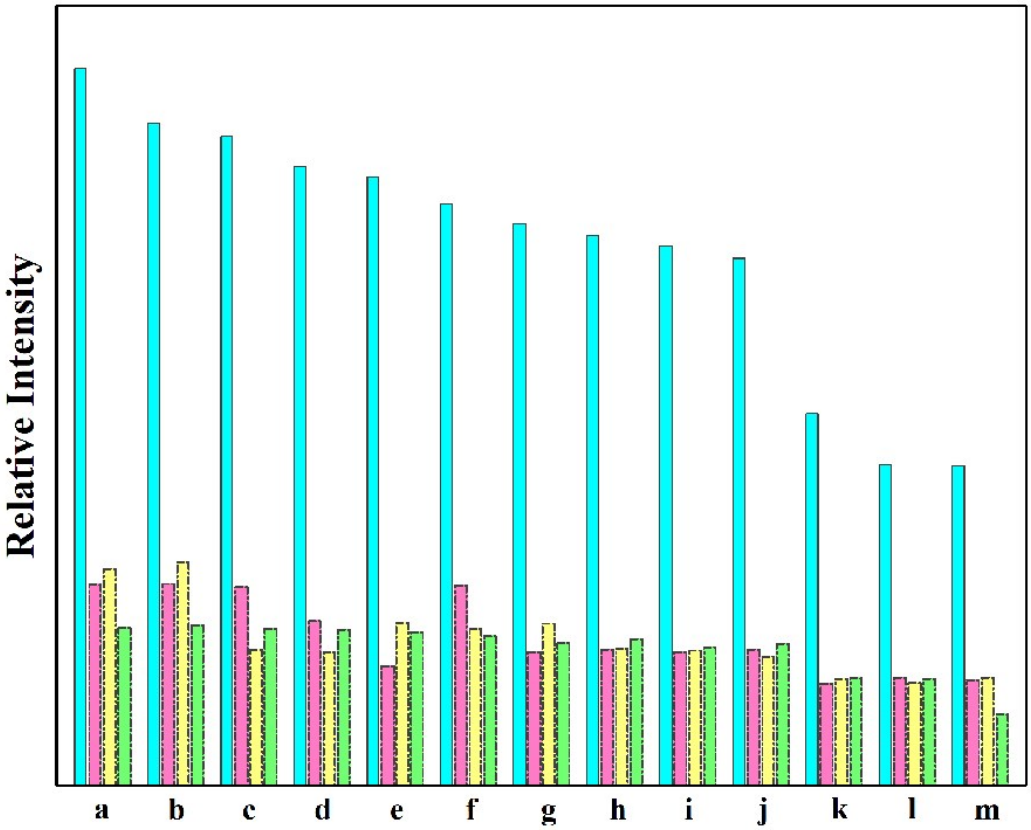

Fig. S27 The bar chart of luminescent intensities at maximum emission wavelength (*ca.* 436 nm) of USTC-5 suspended in 0.01 M interfering anion ion aqueous solutions (blue-green), and in the mixed aqueous solutions including 7.5×10^{-3} M interfering anion ion and 2.5×10^{-4} M $Cr_2O_7^{2-}$ (pink)/CrO_4^{2-}(yellow)/MnO_4^- (green). The interfering anion ion: HCO_3^-(a), SCN^-(b), SO_4^{2-}(c), BrO_3^-(d), Cl^-(e), Br^-(f), NO_3^-(g), ClO_3^-(h), OAc^-(i), CO_3^{2-}(j), I^-(k), $C_2O_4^{2-}$(l) or $H_2PO_4^-$(m).

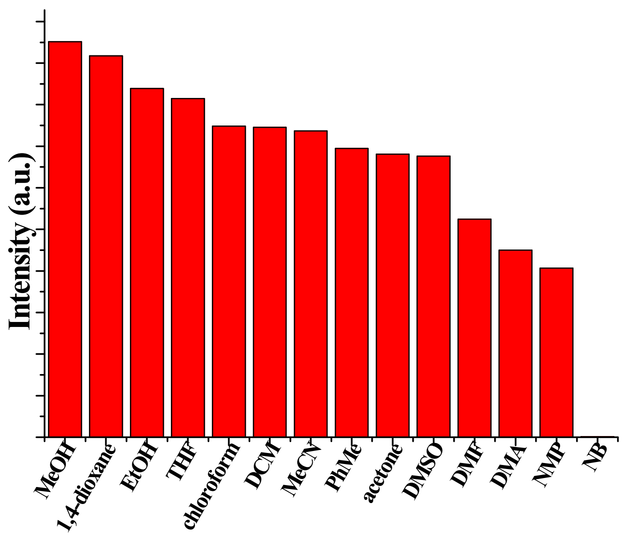

Fig. S28 The bar chart of luminescent intensities at corresponding maximum emission wavelength (407~443 nm) of USTC-5 suspended in different solvents.

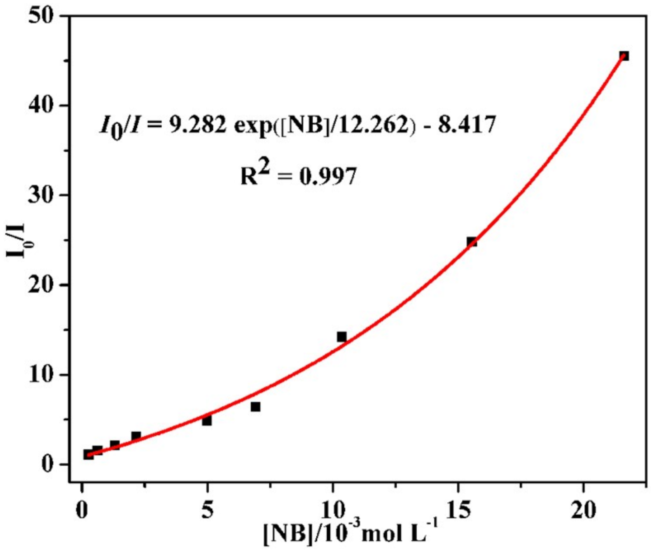

Fig. S29 Plot of I_0/I versus concentration of NB's DMF solutions.

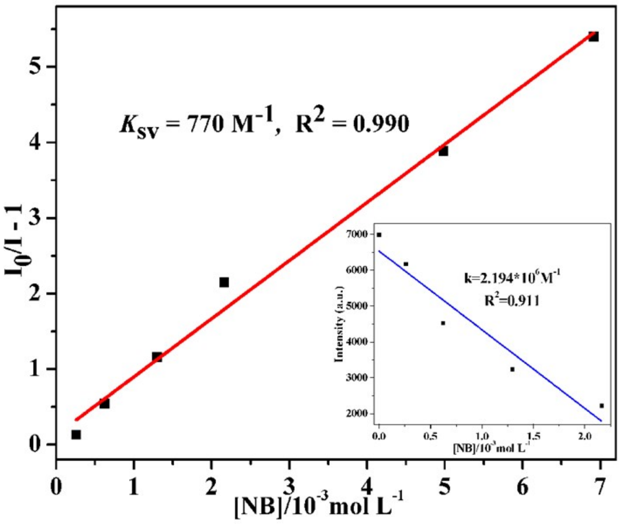

Fig. S30 Stern–Volmer plot of $I_0/I-1$ versus concentration of NB's DMF solutions. Inset: luminescent intensity versus concentration of NB molecule DMF solutions.

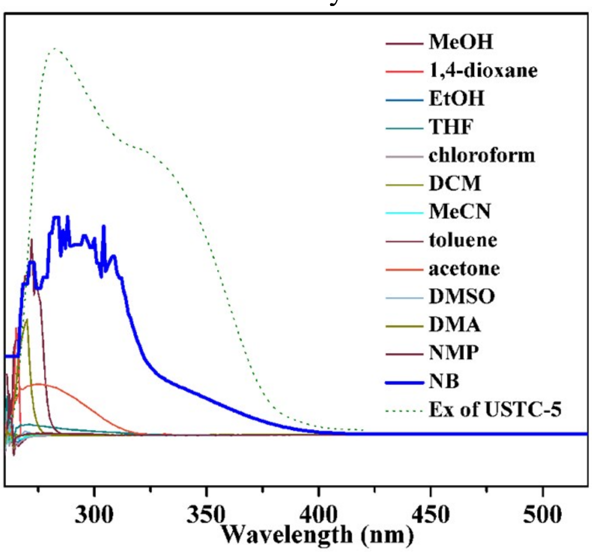

Fig. S31 UV-vis adsorption spectra of USTC-5 dispersed in different solvents, and the excitation spectrum of USTC-5.

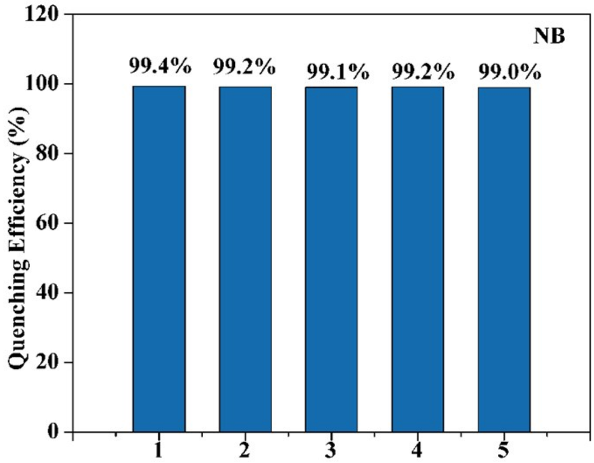

Fig. S32 Quenching efficiencies of USTC-5 in recyclable experiments for NB molecule.

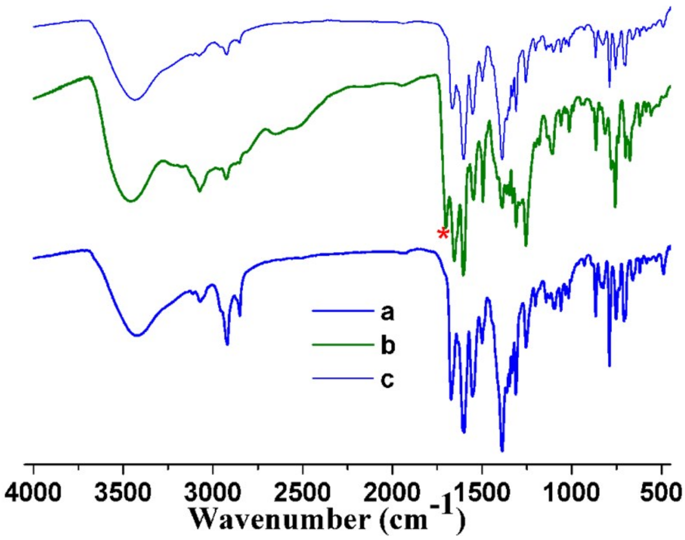

Fig. S33 IR absorption of USTC-5 (a), USTC-5 stimulated by HCl vapor (b), and then stimulated by NH_3 vapor (c). The "C=N+" stretching vibration of the protonated 2-chloroimidazo[1,2-*a*]pyridine rings is marked by asterisk.

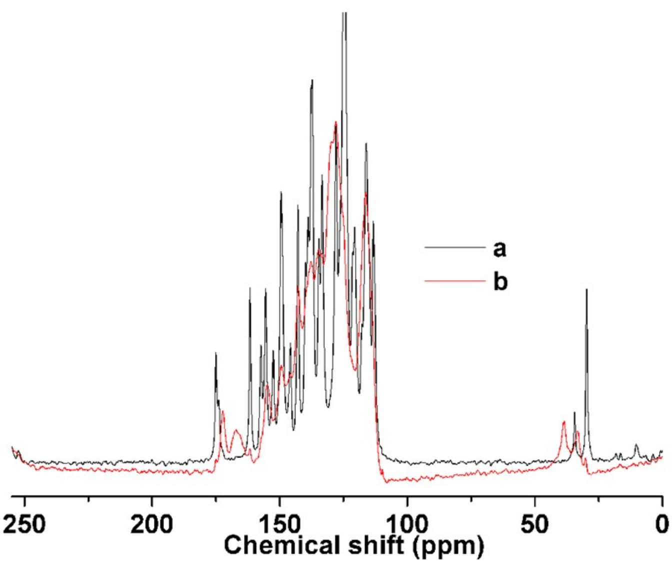

Fig. S34 ^{13}C solid-state NMR spectra of USTC-5 (a) and HCl vapor-disposed USTC-

5 (b).

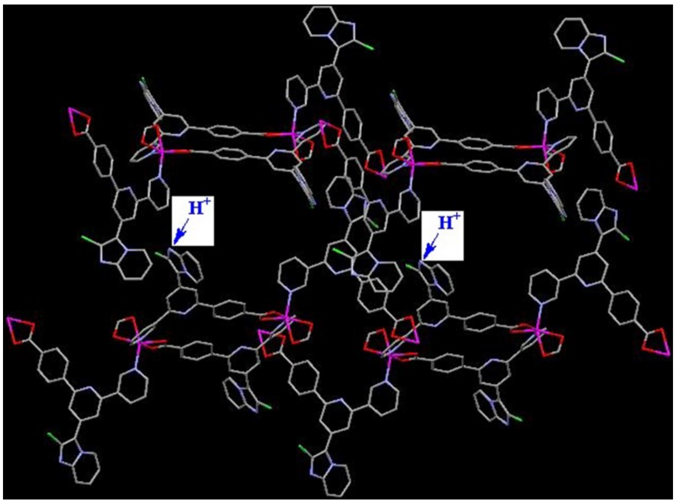

Fig. S35 The protonation of 2-chloroimidazo[1,2-*a*]pyridine rings in USTC-5 by HCl vapor.

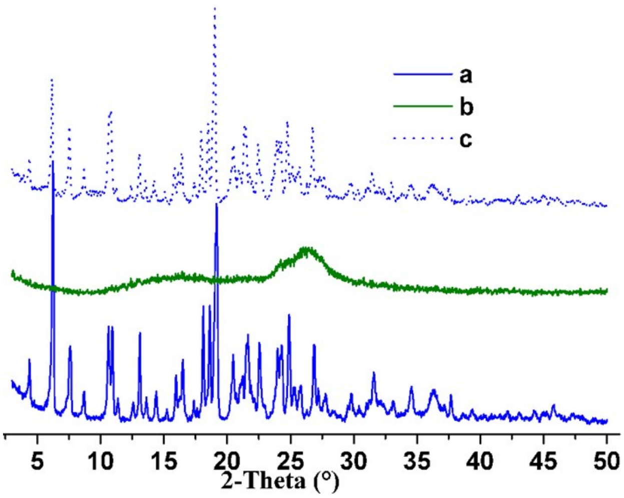

Fig. S36 PXRD patterns of USTC-5 (a), USTC-5 stimulated by HCl vapor (b), and then stimulated by NH_3 vapor (c).